NEW DEVELOPMENTS IN LIDAR UAS SURVEYS. PERFORMANCE ANALYSES AND VALIDATION OF THE DJI ZENMUSE L1.

L. Teppati Losè [1]*, Francesca Matrone [2,3], F. Chiabrando [1], F. Giulio Tonolo [1] , A. Lingua [2], P. Maschio [2]

[1] LabG4CH, Department of Architecture and Design (DAD) - Politecnico di Torino, Viale Mattioli 39, 10125 Torino (Italy) (lorenzo.teppati, filiberto.chiabrando, fabio.giuliotonolo)@polito.it
[2] Laboratory of Photogrammetry, Geomatics & GIS, Department of Environment, Land and Infrastructures Engineering (DIATI) - Politecnico di Torino, Corso Duca degli Abruzzi 24, 10129 Torino (Italy), (andrea.lingua, paolo.maschio,francesca.matrone)@polito.it
3 Department of Structural, Geotechnical and Building Engineering (DISEG) - Politecnico di Torino, Corso Duca degli Abruzzi 24, 10129 Torino (Italy)

ICWG I/II

KEY WORDS: UAS, LiDAR, SfM, 3D, Survey, Accuracy assessment

ABSTRACT:

Thanks to the latest technological developments LiDAR (Light Detection And Ranging) sensors are no longer an exclusive feature of manned airborne platforms but they are close to becoming a commercial solution in the UAS (Uncrewed Aerial Systems) domain. The release on the market of the Zenmuse L1 by DJI (Dà-Jiāng Innovations) is a step further in this direction, thanks also to a substantial work of enhancement made by the Chinese company not only on the hardware side, but also on the software one. The research presented in this work is focused on the use of the L1 LiDAR for the 3D survey of built heritage, analysing the results of different tests to highlight first considerations on its performances and the point cloud quality. Considering its recent release, this sensor is still yet to be thoroughly analysed and validated and its performances to be assessed. LiDAR data has been acquired on a selected test site, documented also with traditional Terrestrial Laser Scanner (TLS) and UAS photogrammetry. The latter techniques (supported also by a topographic survey) will thus be exploited to generate the ground reference and to assess the quality and accuracy of the L1 dataset.

1. INTRODUCTION

The use of LiDAR (Light Detection And Ranging) sensors for aerial acquisitions is generally related to manned aircraft and confined to acquisitions of large portions of land or urban areas. Airborne LiDAR data can be used in different scenarios, e.g. for the automatic extraction of buildings in urban areas (Li et al., 2019), forestry inventory (Webster et al., 2020), and environmental monitoring (Görüm, 2019). Needless to say, acquisitions with this kind of sensors are generally expensive and are usually commissioned by public entities for the monitoring and management of large areas of the territory, and cartography update.

However, in the last years, thanks to the development and diffusion of UAS (Uncrewed Aerial System), new emphasis has been put on the possibility of using LiDAR sensors as UAS payload (Guan et al., 2021; Lin et al., 2021; Troy et al., 2021). The advantages of this approach are evident from the operational point of view due to the intrinsic features of UAS: low-cost (traditional airborne acquisitions are generally expensive), flexibility (easier to transport and deploy on the field), the possibility of off-nadir acquisitions enabled by the gimbal system, possibility of operating in new scenarios (forestry inventory or night-time acquisitions), and finally accessibility to a wider spectrum of operators.

The disadvantages of using LiDAR sensors on UAS are quite evident as well: these kinds of miniaturized LiDAR sensors were quite expensive (until today) with respect to other types of imaging sensors. Moreover, the operational range is shorter compared to the sensors used in airborne acquisitions, the area surveyed with a single acquisition is smaller and the point cloud density is generally lower.

2. MATERIALS AND METHODS

Among the different hardware solutions developed in the last years (Esposito et al., 2014; Gottfried et al., 2015) it is of particular interest the new sensor presented by DJI in October 2020, the Zenmuse L1 (main specifications are reported in Table 1 and an image of the sensor is shown in Figure 1 -a). One of the most interesting features of this sensor is the integration between the LiDAR, the RGB camera and the IMU (Inertial Measurement Unit) module in one single hardware mounted on a 3-axis stabilized gimbal.

LiDAR sensor	
Range	450 m @ 80% reflectivity, 0 klx 190 m @ 10% reflectivity, 100 klx
Point Rate	Single return: max. 240,000 pts/s Multiple return: max. 480,000 pts/s
Positional accuracy	Horizontal: 10 cm @ 50 m Vertical: 5 cm @ 50 m
Point Cloud Coloring	Reflectivity, Height, Distance, RGB
Ranging Accuracy	3 cm @ 100 m

* Corresponding author

FoV	Non-repetitive scanning pattern: 70.4° (horizontal) × 77.2° (vertical) Repetitive scanning pattern: 70.4° (horizontal) × 4.5° (vertical)
Yaw Accuracy	Real-time: 0.3°, Post-processing: 0.15°
Pitch / Roll Accuracy	Real-time: 0.05°, Post-processing: 0.025°
RGB sensor	
RGB camera	1" CMOS 20 MP
Focal Lenght	8.8 mm / 24 mm (Equivalent)

Table 1. DJI Zenmuse L1 main specifications. Full specifications available at: https://www.dji.com/uk/zenmuse-l1/specs

(a) (b)

Figure 1. The Zenmuse L1 (a) and the system mounted as payload with the DJI Matrice 300 (b).

According to the information provided by the manufacturer, this system is capable of acquiring up to 2 km^2 per single flight and can be used with the DJI Matrice 300 UAS (Figure 1 - b) that is provided with an RTK (Real Time Kinematic) module, enabling a direct georeferencing of the acquired data with a claimed accuracy of few centimetres[1].
The performances of this sensor, its metrical and geometrical accuracy, the best operational strategies for data acquisition and processing are still being analysed and validated by different research groups. A first contribution in this sense is reported in a recent work by Štroner et al. (Štroner et al., 2021) that performed different tests on the accuracy of the point cloud acquired with an L1 module and confirmed the potential of such sensor and the needs of further testing. This research group used as test site an area with different features (a building materials landfill) and performed flights at different elevation starting from 50 m a.g.l. (above ground level). The work presented here is focused on a single building and the acquisitions with the L1 were performed at a lower height (35 m a.g.l).
The choice of selecting a single building was related to the aim of testing the performances of the L1 at an architectural scale and with respect to more consolidated survey approaches (TLS and UAS photogrammetry).
The test site is represented by a building in the municipality of Oulx (Torino, North-west Italy) that will become a shelter for migrants.
The building was surveyed during a two days campaign that involved the DIRECT Team (Disaster Recovery Team - https://www.g4ch.polito.it/wordpress/team-direct/), a team of students from the Bachelor and Master degree courses of Architecture and Engineering and that contributed to the data processing phase and the design of the community spaces for the renovation of the building.

2.1 Data acquisition and processing

The fieldwork activities were planned and carried out according to consolidated approaches with the aim to achieve a multi-scale and multi-sensor documentation of the building and its appliances.
First of all, a topographic network was created and measured by means of traditional topographic techniques to georeference all the acquired datasets in the same coordinate system and to measure a series of Ground Control Points (GCPs) and Check Points (CPs) for the metric evaluation of the acquisitions and the different achieved analyses. The network was measured both with Total Station (TS) and Global Navigation Satellite System (GNSS) receivers; the GCPs/CPs were homogeneously distributed all over the surveyed area and were constituted by artificial targets as well as natural features.
Therefore, the terrestrial LiDAR dataset was acquired with a Faro Focus^{3D} X330 (main specifications in Table 2), ensuring a sufficient overlap between scans and a constant distance with respect to the building. The time needed for TLS acquisition was around 3 and an half hours.

Faro Focus^{3D} X330	
Range	0.6-330 m
Measurement speed	~ 976.000 points/s
Ranging error	± 2mm
FoV (vertical/horizontal)	300°/360°

Table 2. Faro Focus^{3D} X330 main specifications.

Scans were then registered using the dedicated software solution Faro SCENE, following a two-step registration approach: a Cloud to Cloud (C2C) registration via the Iterative Closest Point (ICP) algorithm followed by a georeferentiation of the data thanks to a set of GCPs measured by TS. The ICP registration has an error of few millimetres while the target-based one of a couple of centimetres.
Finally the aerial acquisitions were carried out using the Matrice 300 RTK erquipped by two different payloads: the Zenmuse P1 and the Zenmuse L1.
For both the data acquisitions were collected manually due to the conformation of the area, the environmental conditions and the close presence of other buildings; for all these reasons it was necessary to ensure a higher control of the operator over the acquisition and manual flights were preferred to the automatic ones.
Nevertheless, standard guidelines for data acquisition were followed ensuring sufficient overlap (between images for the P1 and between the various scanning lines for the L1), using different sensor's orientations thanks to the 3-axis gimbal (nadir and oblique) and adopting different flight line orientations with respect to the object conformation.
The Zenmuse P1[2] is a full-frame camera developed as payload for the Matrice 300, it has 45MP and a 4.4 µm pixel size: for these acquisitions the 35 mm lens was used and flights were performed at 35 m a.g.l., with an estimated Ground Sample Distance (GSD) of 1 cm/pixel. The total time needed for the flight with the P1 was 20 minutes.
Data were processed using the commercial software solution Agisoft Metashape, based on the standard Structure from Motion (SfM) pipeline, and the main results are reported in Table 3.

[1] Main specifications here: https://www.dji.com/uk/matrice-300?site=brandsite&from=nav

[2] Main specifications here: https://www.dji.com/uk/zenmuse-p1

Images	*GCPSs (6)* *3D RMSe (m)*	*CPs (5)* *3D RMSe (m)*	GSD
423	0.007	0.018	1 cm/pixel

Table 3. Zenmuse P1 main processing results

The acquisitions with the L1 were completed following the same scheme used for the flight with the P1. For this sensor, it was particularly useful to use the real-time visualization of the point cloud during the acquisition in order to ensure adequate coverage of the whole building and avoid areas of missing data.
For the L1 acquisitions the direct georeferencing approach using the RTK capabilities of the Matrice 300 was employed, flights with the L1 were completed in around 10 minutes.
Data were then processed inside the dedicated solution DJI Terra, however, the user's intervention is quite limited and the processing is only partially customizable.
An issue that emerged during the processing was related to the RGB quality of the L1 point cloud that, due to the environmental conditions during the acquisition, resulted quite dark. L1 point cloud is texturized with the images acquired simultaneously to the laser data and that were underexposed in this case (most probably due to the meteorological conditions and the presence of snow coverage). A workaround was used to solve this issue: images radiometry (mainly exposure and contrast) was corrected for each image in an external software and original images were substituted before the processing in DJI Terra. The impact on the RGB quality of the final point cloud is clearly visible in Figure 2.

Figure 2. Radiometric information enhancement. Point cloud processed with acquired images (a) and after image correction (b).

2.2 Methodological approach for comparison analyses

After the processing of the L1 data, different analyses were carried out on the point cloud using third part software solutions such as CloudCompare and Cyclone 3DR. The LiDAR point cloud was analysed following different criteria and adopting different methodologies, using 3D data acquired with other sensors and higher positional accuracies as ground reference in order to evaluate the 3D accuracy, the geometrical resolution and the level of detail.
A Cloud to Cloud (C2C) distances analysis was performed on selected areas of the building: the roof and two of the four facades (north and west). The ground reference for the roof was represented by the point cloud of the Zenmuse P1, while for the two facades both the P1 and TLS datasets were used as references.
Moreover, on some portions of the point cloud a density and roughness analysis were completed using the opensource solution CloudCompare. As regards the density analysis, the surface density and number of neighbors were estimated with a sphere of radius 0.04 m, corresponding to the accuracy for a final representation scale of 1:100 (according to commonly adopted Italian standards). In particular, an area on the west façade was chosen for the L1, P1 and TLS, while on the roof only the P1 and L1 were compared, due to the lack of data for the TLS (Figure 3a). For the roughness a radius of 0.1 m was selected on roof pitches' intersection and facades with windows (Figure 3b).

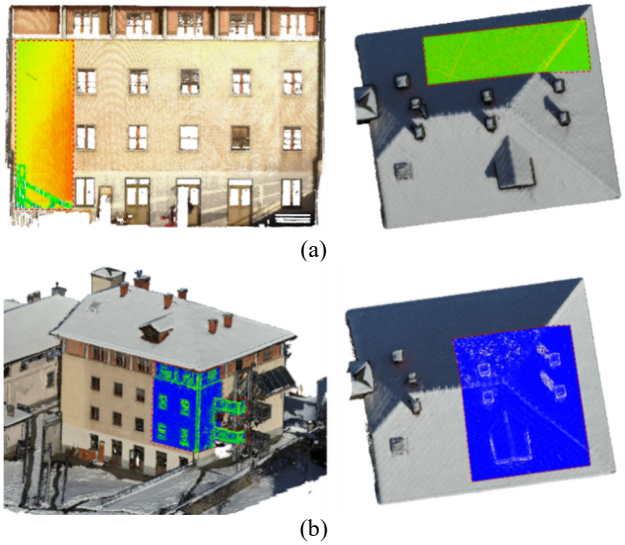

Figure 3. Selected areas on the façade (a) and the roof (b) for the density analysis.

Given the ever increasing trend on point cloud semantic segmentation, based on the use of 3D geometric features with ML algorithms (Grilli et al., 2021; Matrone et al., 2020), further tests also investigated whether the L1 point clouds could be appropriate for this task, computing a few 3D features, such as verticality (radius 0,1 m), omni-variance (radius 0,2 m) and surface variation (radius 0,1 m). The choice of the radius is determined by the ability of the feature to properly discriminate the various architectural elements (façades, windows, roofs and so on).

3. RESULTS

3.1 C2C analyses

The first C2C analysis was completed on the roof of the building, where P1 point cloud was used as reference. Results are reported in Figure 4 and Table 4.

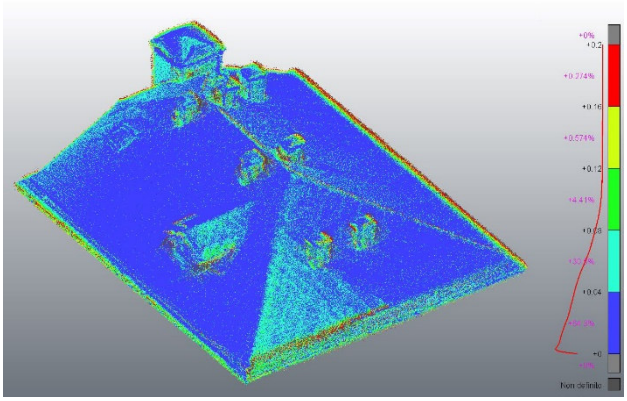

Figure 4. C2C analyses of the roof. P1 is used as ground reference and L1 as compared dataset.

What emerged from this analysis, confirmed by other tests reported hereafter, is that the L1 point cloud is affected by a higher noise if compared with the P1 dataset. This issue is evident

also in the false colours representation, where the sharpest geometric features of the building (e.g. the ridgeline) are the areas where the higher deviation between the two datasets is observable.

C2C analyses for the roof (deviation expressed in m)			
C2C	**0<%<0,04**	**0,04<%<0,08**	**%>0,08**
P1-L1	64,3	30,5	5,2%

Table 4. C2C analyses roof dataset. For each dataset values are reported as percentages in a selection of ranges.

Nevertheless, the distribution of the deviations as reported in Table 4 confirms an overall good performance of the L1 with more than 64 percent of points with a deviation lower than 0,04 m and around 95 percent of points with a deviation lower than 0,08 m. It needs also to be reported that these errors can be related to the presence of snow on the roof and thus further tests are needed in other scenarios with similar environmental conditions. The results of the C2C analysis for the two facades provided slightly different results. For the west façade, different observations can be underlined for the C2C analysis that used the TLS as ground reference and the one using the P1 as ground reference. In this case, the façade is characterised by several windows whose geometry was only partially described from both the terrestrial and aerial acquisitions. The upper part of windows frames was acquired by the TLS, while the lower part from the UAS acquisitions depending on the acquisition geometry. For this reason, these areas are the ones with the higher deviation between the L1 dataset and the reference models (Figure 5).

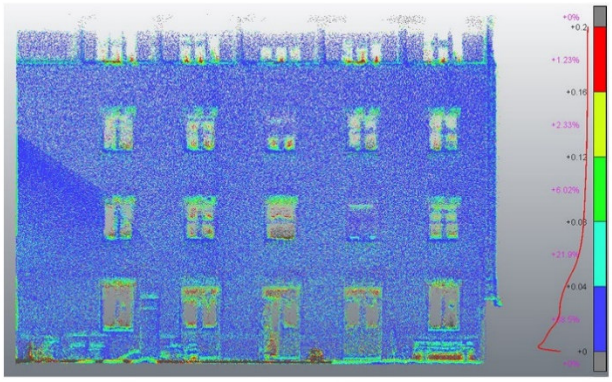

(a) TLS-L1

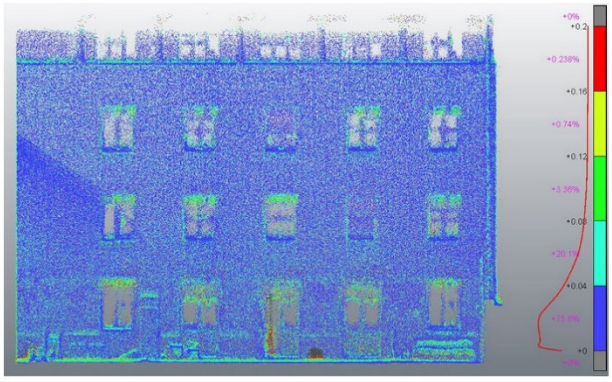

(b) P1-L1

Figure 5. C2C analyses of the west facade. TLS (a) and P1 (b) are used as ground reference and L1 as compared dataset.

Data reported in Table 5 confirms that the C2C analysis using different datasets as ground reference provides comparable results. It is observable a slightly higher number of points with deviation lower than 0,04 meters in the case of P1-L1 analysis; this can be ascribed again at the acquisition geometry (both are aerial acquisitions) and thus the sensors' position and orientation with respect to the building. Nevertheless, for both the dataset more than 90% of points present deviations lower than 0.08 meters.

C2C analyses for the west façade (deviation expressed in m)			
C2C	**0<%<0,04**	**0,04<%<0,08**	**%>0,08**
TLS-L1(a)	68,5	21,9	9,6
P1-L1 (b)	75,6	20,1	4,3

Table 5. C2C analyses of the west facade. For each dataset values are reported as percentages in a selection of ranges.

The same analysis has been carried out on the north wall: results are reported in Figure 6 and Table 6. Compared to the other datasets, the one of the north façade presents a higher percentage of points with a deviation bigger than 0,08 m: however, the localization of these points is clearly visible in the false colours representation. The error is located on the floor in front of the façade that was a crossing point during the acquisitions and that was covered by snow. Due to the modifications derived from people's walking on the snow between the different acquisitions this area is affected by higher deviations. On the façade it is possible to remark the same issue encountered for the roof concerning the noise. Also in this case, due to the noise of the L1 dataset, sharper geometry presents a higher deviation with respect to the reference dataset.

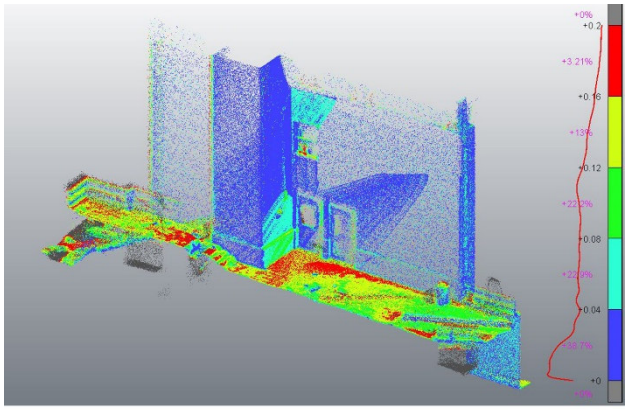

(a) TLS-L1

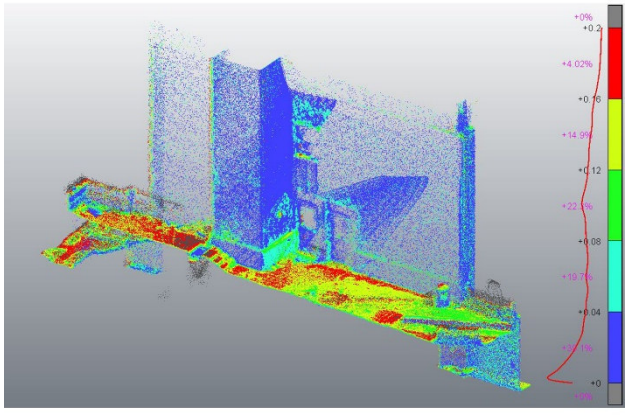

(b) P1-L1

Figure 6. C2C analyses of the north façade. TLS (a) and P1 (b) are used as ground reference and L1 as compared dataset.

C2C analyses for the north façade (deviation expressed in m)			
C2C	**0<%<0,04**	**0,04<%<0,08**	**%>0,08**
TLS-L1(a)	38,7	22,9	38,4
P1-L1 (b)	39,1	19,7	41,2

Table 6. C2C analyses of the north facade. For each dataset values are reported as percentages in a selection of ranges.

3.2 Density analyses

The first density and neighbors analyses were performed on a part of the west façade, where TLS point cloud was used as reference. As shown in Figure 7 and Table 7 the TLS and P1 point clouds are respectively denser than the L1 one. Approximately 50% of the points has the number of neighbors lower than 48 points for the TLS, 31 points for the P1 and 13 points for the L1.

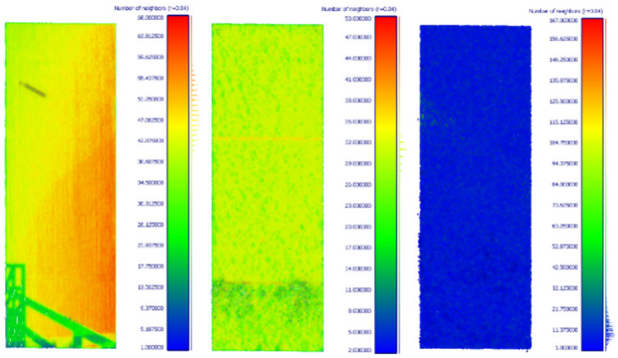

(a) TLS **(b) P1** **(c) L1**

Figure 7. Density analyses of a west façade section. The color scale on the right of each image is proportional to the number of neighbors, while the image represents the density visualization..

Number of neighbors for a sample of the west façade (radius 0,04 m)			
	Nr. of points	**Mean**	**St. deviation**
TLS	270.645	47,42	7,22
P1	179.357	29,87	3,32
L1	162.506	21,12	20,69
Surface density* for a sample of the west façade (radius 0,04 m)			
	Nr. of points	**Mean**	**St. deviation**
TLS	270.645	9433,14	1436,84
P1	179.357	5943,61	661,39
L1	162.506	4202,12	4116,67

Table 7. Density analyses of the west façade section.
*number of neighbors (N) divided by the neighborhood surface: $N/(\pi r^2)$

Opposite behaviour is encountered for the roof area analysed.
In this case, the TLS point cloud was not considered for the obvious lack of data, nevertheless the P1 constitutes a proper reference for the comparison.
As it is possible to notice from Figure 8 and Table 8, the number of points of the selection of L1 point cloud is almost 3 times the one of the P1. However, the mean of the L1 surface density is not heavily higher if compared to the P1. This result could be due to the inhomogeneity of the points' distribution, namely their roughness; for this reason, it was considered appropriate to carry out the test described in paragraph 3.3.

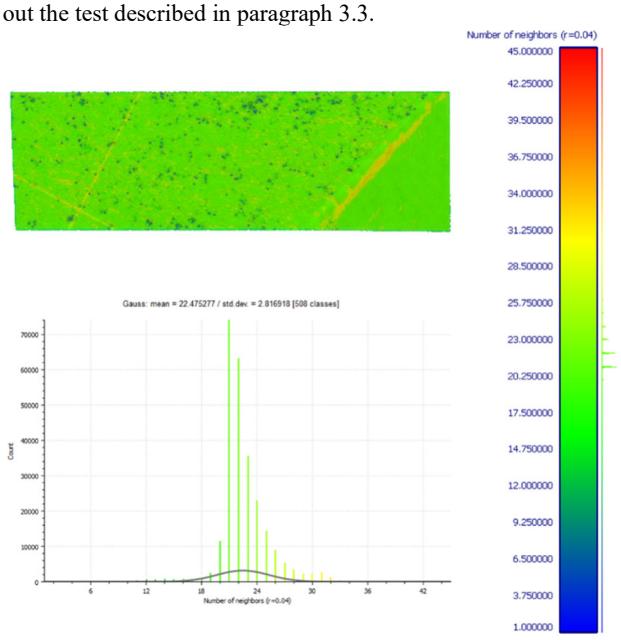

(a) P1

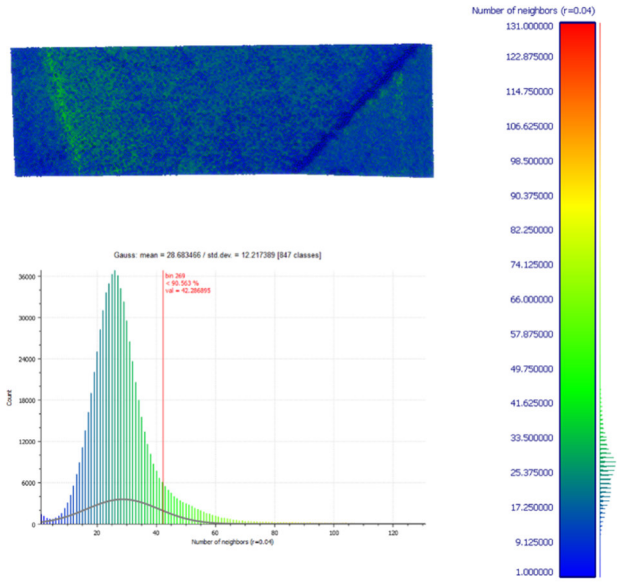

(b) L1

Figure 8. Density analyses of a roof section. The color scale on the right of each image shows the number of neighbors, while the image represents the density visualization. P1 (a) is used as ground reference and L1 (b) as compared dataset.

Number of neighbors for a sample of the roof (radius 0,04 m)			
	Nr. of points	**Mean**	**St. deviation**
P1	257.450	22,47	2,82
L1	716.252	28,68	12,22
Surface density* for a sample of the roof (radius 0,04 m)			
	Nr. of points	**Mean**	**St. deviation**
P1	257.450	4471,31	560,41
L1	716.252	5706,39	2430,57

Table 8. Density analyses of the roof section.
*number of neighbors (N) divided by the neighborhood surface: $N/(\pi r^2)$

3.3 Roughness analyses

Based on the results of the previous section, an in depth analysis of the point cloud roughness on a sample of the roof was performed. In particular, the intersection between the roof pitches, including also the chimneys and dormers, was firstly selected. The roughness represents the surface complexity (Milenković et al., 2013) and it corresponds to the distance between the considered point and the best fitting plane computed on its nearest neighbors (cloudcompare.org).
Figure 9 and Table 9 clearly confirm how L1 presents a higher number of points, but also a higher value both for the roughness mean and standard deviation. This outcome points out that the greater number of points could be due to the L1 sensor noise, as clearly visible in Figure 10 where it is compared to the P1 point cloud (with a distinctly lower noise, despite the snow coverage).

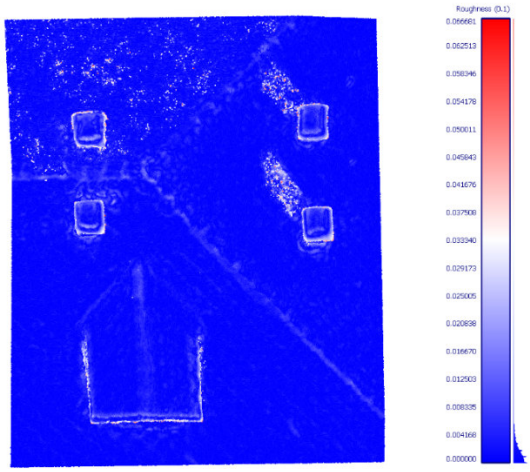

(a) P1

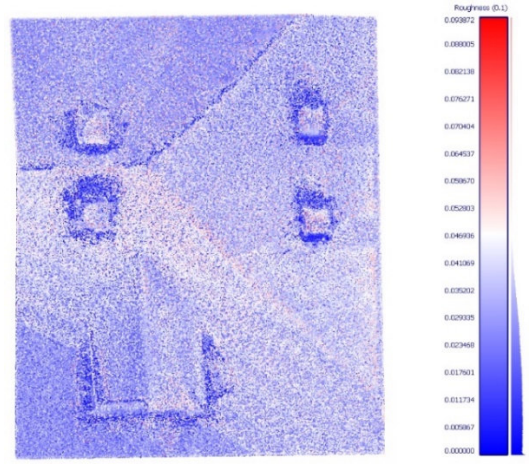

(b) L1

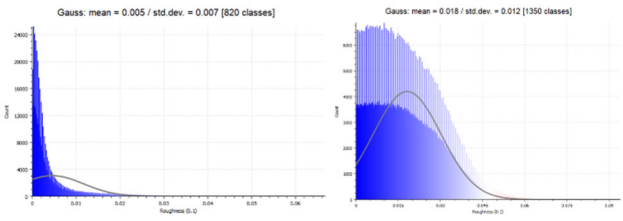

(c)

Figure 9. Roughness analyses of a roof area, computed with a radius of 0,1 m. P1 (a) is used as ground reference and L1 (b) as compared dataset. On the bottom (c), the gaussian distribution for P1 on the left and L1 on the right.

Roughness for a sample of the roof (radius 0,1 m)			
	Nr. of points	**Mean (m)**	**St. deviation (m)**
P1	671.500	0,005	0,007
L1	1.821.304	0,018	0,012

Table 9. Roughness analyses of the roof section.

Figure 10. Comparison between P1 (on the left) and L1 (on the right).

Similar results were obtained for the façade, where also the emergency stairs have been included. Figure 11, b clearly depicts how the P1 has some weaknesses on the stairs and the discontinuity planes (e.g. windows and gutters), while the L1 Figure 11, c) mixes all the elements without an effective distinction.

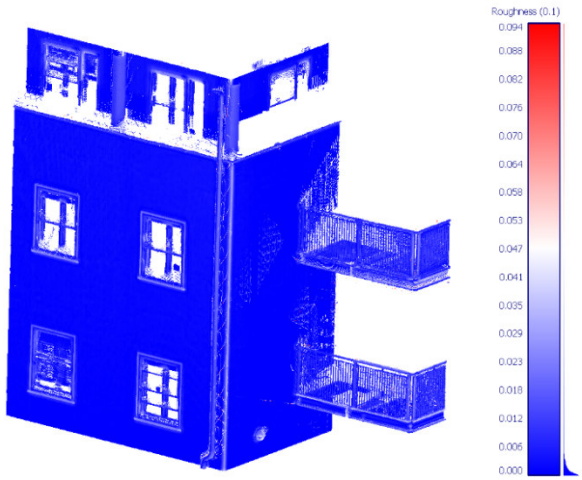

(a) TLS

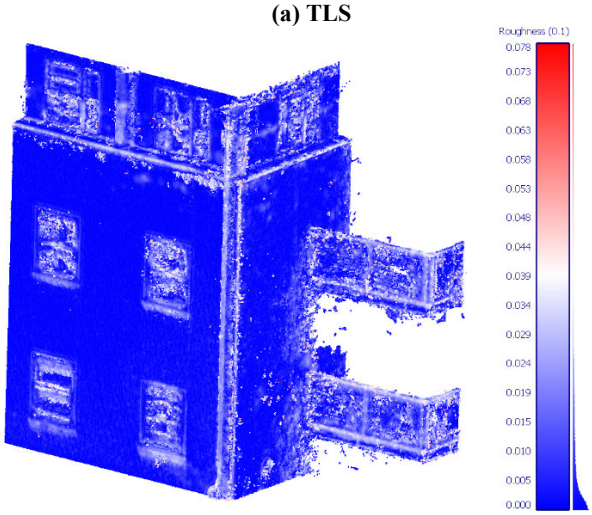

(b) P1

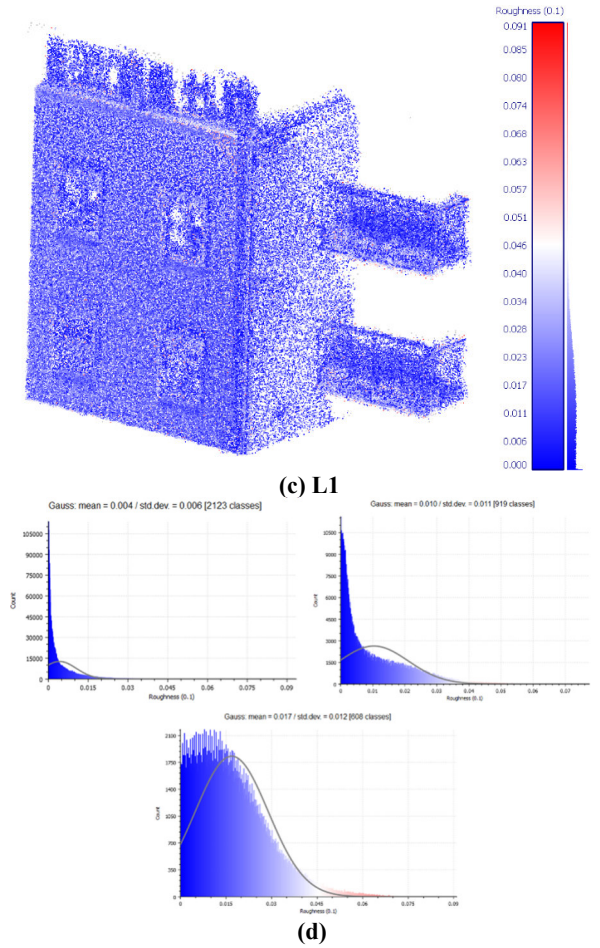

Figure 11. Roughness analyses of the façade section, computed with a radius of 0,1 m. TLS (a) and P1 (b) are used as ground reference and L1 (c) as compared dataset. On the bottom (d), the gaussian distribution for TLS on the top left, P1 on the top right and L1 in the centre.

Roughness for a sample of the west façade (radius 0,1 m)			
	Nr. of points	**Mean (m)**	**St. deviation (m)**
TLS	4.503.236	0,004	0,006
P1	842.924	0,010	0,011
L1	369.293	0,017	0.12

Table 10. Roughness analyses of the façade section.

3.4 Qualitative analysis and 3D features extraction

To test the effectiveness of the use of the L1 sensor also for the point cloud classification and semantic segmentation tasks (based on Machine Learning -ML alghoritms), some 3D features have been computed. This analysis has been carried out as a qualitative test and is not to be intended as exhaustive.

In particular, the verticality, the omnivariance and the surface variation have been selected both for the P1 and the L1 sensors. As it can be noticed from Figure 12, to obtain comparable results for similar inputs to the ML algorithms, it has been necessary to vary the computation radii for the L1-based inputs. Thanks to this change the final L1 features can discriminate likewise those of the P1.

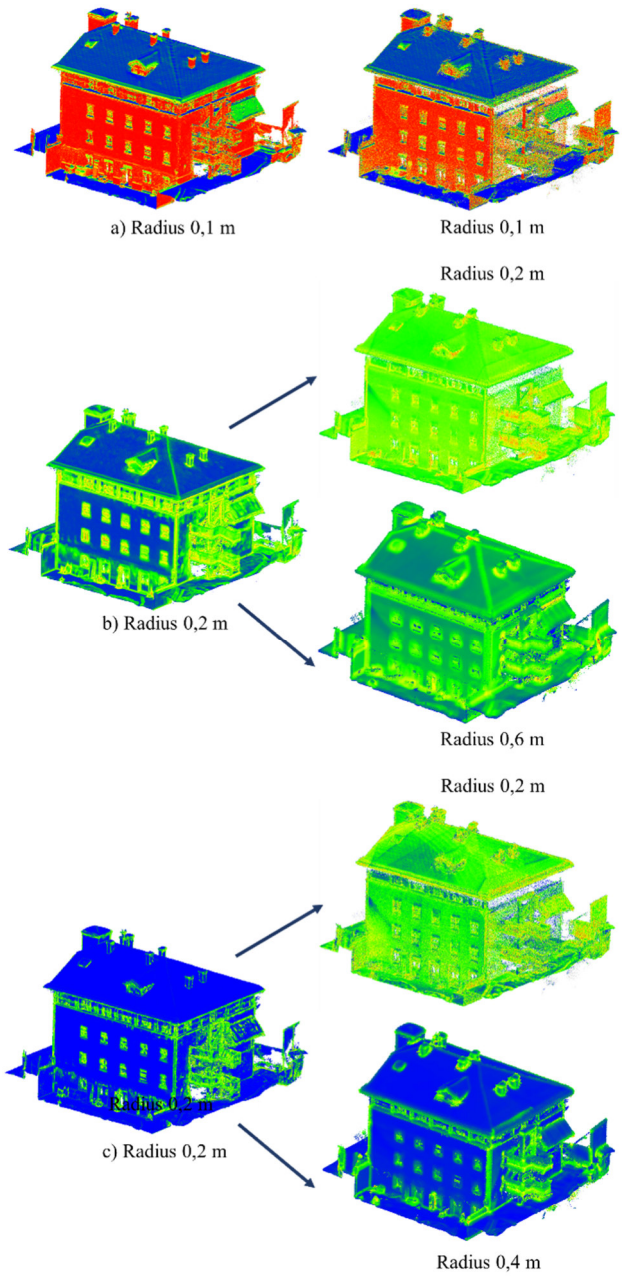

Figure 12. Geometric features computed for the P1 (on the left) and L1 (on the right) point clouds. Verticality (top, a), omnivariance (centre, b) and surface variation (bottom, c).

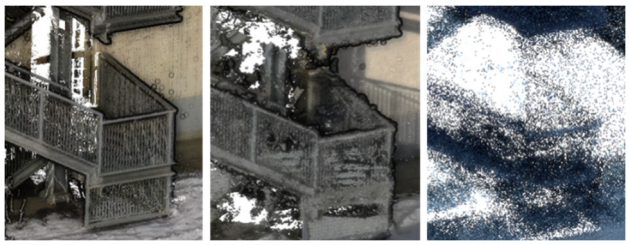

Figure 13. Emergency stairs detail on the south façade. TLS (a), P1 (b), L1 (c).

Finally, Figure 13 depicts the emergency stairs of the south façade. In this case, it results clear the noise of the L1 point cloud

and its limits in achieving a satisfactory level of detail for this kind of element.

4. DISCUSSION AND CONCLUSIONS

The test and analyses presented in this work allow to confirm the overall good performances of the Zenmuse L1 for the survey of the built heritage. The first aspect that can be underlined is connected to the rapidity and easiness of data acquisition. The L1 can be easily deployed in the field together with the Matrice 300 and data acquisition can be performed in few minutes. Compared with other surveys techniques the cost-benefit ratio is definitely low. However, the quality of the collected data needs to be accounted for as well. In this sense, the L1 has the lowest performances in terms of level of detail of the 3D data and related noise. The analysis achieved confirmed that TLS and aerial photogrammetry have still the upper hand in the definition of the object's geometries.
Another issue that must be accounted for is related to the quality of the visible images acquired by the L1 sensor. In case of unfavourable environmental conditions or error in the setup of camera parameters during the acquisition, a pre-processing of the images is feasible and can improve the final radiometric content of the point cloud.
Concerning the processing, the L1 dataset was the fastest one in terms of processing time. The P1 dataset requires more computational time while the TLS required both more human effort and processing time (for point cloud registration, filtering, and segmentation).
The aforementioned considerations need to be carefully assessed in relation to the nominal scale requested from the survey. Nevertheless, the resolution and precision of the L1 point cloud are generally sufficient to cover the requirements of the standard architectural representation (1:100/1:200). Results are particularly interesting considering the operative condition during the acquisition on the test site (e.g. the presence of snow).
A missing step in the DJI Terra processing is related to the possibility to import and use GCPs as independent elements to metrically validate the L1 dataset. In this sense, further tests on the use of specific targets with high reflectivity can be planned to streamline the identification of GCPs in the point cloud.
An interesting feature of the L1 is connected with the availability of 3 different returns signals that can be exploited especially for forestry inventory or landscape survey activities and that will need further investigation (including the possible impact when surveying snow-covered areas)
The density and roughness analyses highlighted some criticalities of the L1, when dealing with architectural details or discontinuity areas. Moreover, the higher number of points on the roof did not implied a higher accuracy: on the contrary, it was demonstrated how this outcome was related to the noise of the point cloud. Nevertheless, the effective results of the 3D features computation make L1 point clouds suitable for the classification and semantic segmentation tasks, proving that this sensor can be properly used for urban and architectural applications.

REFERENCES

Esposito, S., Mura, M., Fallavollita, P., Balsi, M., Chirici, G., Oradini, A., & Marchetti, M. (2014). Performance evaluation of lightweight LiDAR for UAV applications. *International Geoscience and Remote Sensing Symposium (IGARSS)*, 792–795. https://doi.org/10.1109/IGARSS.2014.6946543

Görüm, T. (2019). Landslide recognition and mapping in a mixed forest environment from airborne LiDAR data. *Engineering Geology*, *258*, 105155. https://doi.org/10.1016/J.ENGGEO.2019.105155

Gottfried, M., Hollaus, M., Glira, P., Wieser, M., Riegl, U., & Pfennigbauer, M. (2015). First examples from the RIEGL VUX-SYS for forestry applications. *Proceed. SilviLaser*, 105–107.

Grilli, E., Poux, F., & Remondino, F. (2021). Unsupervised Object-Based Clustering in Support of Supervised Point-Based 3d Point Cloud Classification. *The International Archives of Photogrammetry, Remote Sensing and Spatial Information Sciences*, *43*, 471-478.

Guan, H., Sun, X., Su, Y., Hu, T., Wang, H., Wang, H., Peng, C., & Guo, Q. (2021). UAV-lidar aids automatic intelligent powerline inspection. *International Journal of Electrical Power & Energy Systems*, *130*, 106987. https://doi.org/10.1016/J.IJEPES.2021.106987

Li, M., Rottensteiner, F., & Heipke, C. (2019). Modelling of buildings from aerial LiDAR point clouds using TINs and label maps. *ISPRS Journal of Photogrammetry and Remote Sensing*, *154*, 127–138. https://doi.org/10.1016/J.ISPRSJPRS.2019.06.003

Lin, Y. C., Liu, J., Fei, S., & Habib, A. (2021). Leaf-Off and Leaf-On UAV LiDAR Surveys for Single-Tree Inventory in Forest Plantations. *Drones 2021, Vol. 5, Page 115*, *5*(4), 115. https://doi.org/10.3390/DRONES5040115

Matrone, F., Grilli, E., Martini, M., Paolanti, M., Pierdicca, R., & Remondino, F. (2020). Comparing machine and deep learning methods for large 3D heritage semantic segmentation. *ISPRS International Journal of Geo-Information*, *9*(9), 535.

Milenković, M., Ressl, C., Hollaus, M., & Pfeifer, N. (2013, April). Surface Roughness from Point Clouds-A Multi-Scale Analysis. In *EGU General Assembly Conference Abstracts* (pp. EGU2013-13570).

Štroner, M., Urban, R., Línková, L., Wilkinson, E., Abd-Elrahman, A., & Andrew Lassiter, H. (2021). A New Method for UAV Lidar Precision Testing Used for the Evaluation of an Affordable DJI ZENMUSE L1 Scanner. *Remote Sensing 2021, Vol. 13, Page 4811*, *13*(23), 4811. https://doi.org/10.3390/RS13234811

Troy, C. D., Cheng, Y. T., Lin, Y. C., & Habib, A. (2021). Rapid lake Michigan shoreline changes revealed by UAV LiDAR surveys. *Coastal Engineering*, *170*, 104008. https://doi.org/10.1016/J.COASTALENG.2021.104008

Webster, C., Mazzotti, G., Essery, R., & Jonas, T. (2020). Enhancing airborne LiDAR data for improved forest structure representation in shortwave transmission models. *Remote Sensing of Environment*, *249*, 112017. https://doi.org/10.1016/J.RSE.2020.112017